Typical values of Rietveld instrument profile coefficients

Article *in* Powder Diffraction · March 2011

DOI: 10.1154/1.3548128

CITATIONS
19

READS
9,465

2 authors:

James Kaduk
Illinois Institute of Technology
452 PUBLICATIONS **3,566** CITATIONS

SEE PROFILE

Joel W. Reid
Canadian Light Source Inc. (CLS)
63 PUBLICATIONS **1,634** CITATIONS

SEE PROFILE

Typical values of Rietveld instrument profile coefficients

James A. Kaduk[a)]
Illinois Institute of Technology, 3101 S. Dearborn St., Chicago, Illinois 60616

Joel Reid
International Centre for Diffraction Data, 12 Campus Blvd., Newtown Square, Pennsylvania 19073

(Received 17 September 2010; accepted 26 December 2010)

GSAS instrument parameters are tabulated for a variety of laboratory and synchrotron diffractometers to give users an idea of the typical ranges of profile parameters when they generate their own instrument parameter files. For modern high-resolution laboratory diffractometers, the parameters fall in the ranges $0<U<3$, $V=0$, $0<W<4$, $1<X<3$, $0<Y<3$, $1<\text{asym}<3$, and $0<S/L<0.03$. For synchrotron diffractometers, the parameters fall in the ranges $0<U<1.2$, $-1<V<0$, $0<W<1$, $0<X<1$, $0<Y<1$, $0<\text{asym}<0.5$, $0<S/L<0.001$, and $0<H/L<0.007$. FULLPROF equivalents are also reported. The factors which are convoluted together to generate the instrument profile are described. © *2011 International Centre for Diffraction Data.* [DOI: 10.1154/1.3548128]

Key words: Rietveld, instrument profile, profile function, convolution

I. INTRODUCTION

An aspect of the Rietveld method that can cause anxiety to newcomers is the necessity to describe the peak profile contributions from the specimen and from the instrument. Often one spends more time worrying about the profiles than the structure in a Rietveld refinement. To interpret the observed peak profiles properly, one needs to understand the instrument profile contributions. These instrument contributions are generally characterized by collecting data from a specimen known to exhibit no size or strain broadening [often a National Institute of Standards and Technology (NIST) Standard Reference Material (SRM)].

Over more than 25 years of performing Rietveld refinements, we have characterized many diffractometers in our own laboratories, as well as in other laboratories we have visited. In this paper, we tabulate and discuss these laboratory instrument profile parameters (as well as those from several synchrotron diffractometers), so that new users of the Rietveld method may have some idea of the normal ranges of values.

While numerous Rietveld refinement programs are currently available (Cranswick, 2008), including both freely distributed and vendor software packages, two free programs have attained very widespread usage: GSAS (Larson and Von Dreele, 2004) and FULLPROF (Rodriguez-Carvajal, 2001). The tabulations of instrument profile coefficients in this paper concentrate on these two programs and the relationships between the profile coefficients.

II. X-RAY DIFFRACTION PROFILE SHAPES

To understand X-ray diffraction peak profiles, we need to understand the mathematical operation of convolution. The convolution of two functions (of time, in this example) $f(t)$ and $g(t)$ is defined as

$$(f * g)(t) = \int_{-\infty}^{\infty} f(\tau) \cdot g(t-\tau) d\tau = \int_{-\infty}^{\infty} f(t-\tau) \cdot g(\tau) d\tau, \quad (1)$$

in which τ is an intermediate variable. An excellent discussion of convolution (as well as animated examples) is found in Wikipedia (2010). Convolution is the basis of the fundamental parameter approach (Cheary and Coelho, 1992), and the factors which affect peak profiles can be studied by using ray-tracing programs. The convolution of one function (the input) with a second function (the response function) gives the output of an electrical circuit. In optics, "blur" is described by convolutions, so this mathematics is natural for describing X-ray peak profile functions.

X-ray diffraction peak profiles are complex, and this complexity slowed the application of the Rietveld method to X-ray data. Many factors contribute to this complexity. For the Bragg-Brentano geometry, Klug and Alexander (1974) summarized the main contributions: the X-ray source, the flat surface, the axial divergence, the specimen transparency, and the receiving slit (Table I). More recent and more accessible treatments are found from Le Bail (2008) and Kern (2008). Masson *et al.* (2003) gave a similar discussion for synchrotron profiles.

TABLE I. Contributions to X-ray line profiles (Klug and Alexander, 1974).

Effect	Equation	Range
X-ray source	$\exp(-k_1^2\varepsilon^2)$ $k_1=1.67(\text{FWHM})$	$-\infty$ to $+\infty$
Flat surface	$\lvert\varepsilon\rvert^{-1/2}$	$-(\gamma^2 \cot\theta)/114.6$ to 0 γ=divergence
Axial divergence	$\lvert 2\varepsilon \cot\theta\rvert^{-1/2}$	$-(\delta^2 \cot\theta)/(4\times 57.3)$ to 0 δ=axial divergence
Transparency	$\exp(k_4\varepsilon)$ $k_4=(4\mu R/114.6)\sin 2\theta$	$-\infty$ to 0
Receiving slit		$-(\text{FWHM})/2$ to $+(\text{FWHM})/2$

Note: ε=angle difference from the angle of maximum intensity.

[a)]Author to whom correspondence should be addressed. Electronic mail: kaduk@polycrystallography.com

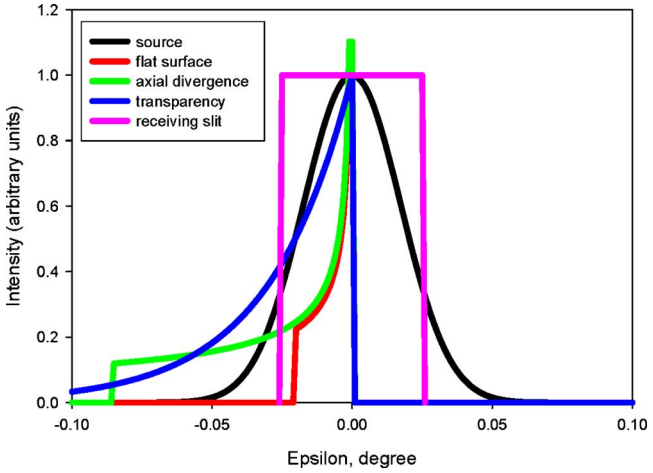

Figure 1. (Color online) Contributions to an X-ray peak profile in the Bragg-Brentano geometry. The curves have been scaled to approximately the same height. The convolution of all five of these functions results in an asymmetric Gaussian profile. Generation of the complete profile requires an additional convolution of the Lorentzian Cu $K\alpha$ emission profile.

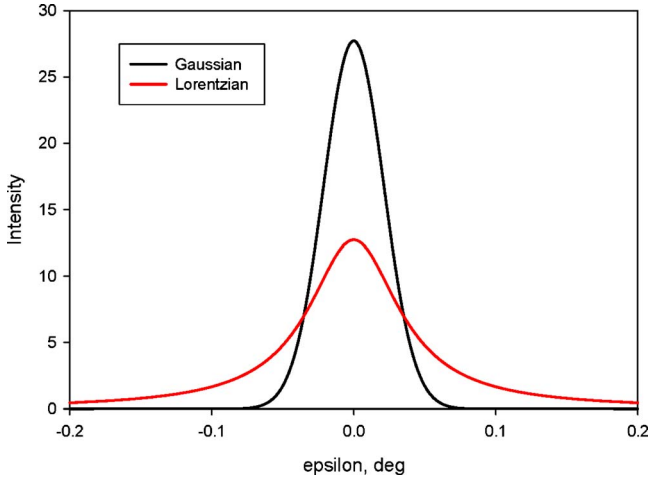

Figure 2. (Color online) These Gaussian and Lorentzian peaks have the same FWHM and area. The Lorentzian peak tails are much wider.

The intensity profile of the X-ray source is generally described well by a Gaussian function (Figure 1). The flat surface, axial divergence, and transparency contributions result in low-angle tails, and the receiving slit is a rectangular window. The convolution of these five effects is an asymmetric Gaussian profile. To obtain the instrumental profile, an additional convolution with the Lorentzian Cu $K\alpha$ emission profile (Hartwig *et al.*, 1993) is required.

The low-resolution neutron diffraction peaks used by Rietveld (1969) in his initial refinements were observed to be Gaussian. Their widths and shapes were determined mainly by the neutron spectral distribution, the monochromator response function (including the mosaic spread of the crystal), and the divergences of the Soller collimators as evaluated by Caglioti *et al.* (1958), resulting in the equation commonly referred to as the "Caglioti" function, which describes the variation in full width at half maximum (FWHM) as a function of diffraction angle,

$$\mathrm{FWHM}^2 = U\tan^2\theta + V\tan\theta + W. \tag{2}$$

This equation does not appear as such in the original paper but was simplified by Rietveld. Equation (2) and derivatives have been used to describe X-ray peak widths by a number of authors but particularly by Cheary and Cline (1995).

Real X-ray diffraction peaks thus contain both Gaussian and Lorentzian components, so it is natural to use combinations of Gaussian [Eq. (3)] and Lorentzian [Eq. (4)] functions (Young, 1993) to describe them,

$$G_{i,k}(2\theta) = [(4\ln 2)^{1/2}/(H_k\pi^{1/2})] \times \exp((-4\ln 2(2\theta_i - 2\theta_k)^2)/H_k^2), \tag{3}$$

$$L_{i,k}(2\theta) = [2/(\pi H_k)]/[1 + \{4(2\theta_i - 2\theta_k)^2/H_k^2\}]. \tag{4}$$

In these equations, $(G,L)_{i,k}$ is the intensity of the ith point of the kth line of the pattern and H_k is the full width at half maximum. The ideal combination would be a Voigt function (convolution of Gaussian and Lorentzian), but for a long time this was too numerically intensive to be practical. Fundamental parameter approaches now compute the convolutions efficiently. The most widely used combination has been the pseudo-Voigt function [a linear combination of Gaussian (G) and Lorentzian (L) profiles]. The pseudo-Voigt function has generally been implemented in one of the two ways. The original version was a simple sum based on an angle-dependent mixing parameter η (Young and Wiles, 1982; Young, 1993),

$$pV = \eta L + (1-\eta)G, \tag{5}$$

$$\eta(2\theta) = \eta_0 + \eta_1 \cdot 2\theta. \tag{6}$$

Subsequently, a second description by Thompson, Cox, and Hastings was developed, a description which explicitly represents the mixing parameter in terms of the Gaussian and Lorentzian FWHM parameters Γ_G and Γ_L (Thompson *et al.*, 1987),

$$\eta = 1.366\ 03(\Gamma_L/\Gamma) - 0.477\ 19(\Gamma_L/\Gamma)^2 + 0.111\ 16(\Gamma_L/\Gamma)^3, \tag{7}$$

$$\Gamma = (\Gamma_G^5 + 2.692\ 69\Gamma_G^4\Gamma_L + 2.428\ 43\Gamma_G^3\Gamma_L^2 + 4.471\ 63\Gamma_G^2\Gamma_L^3 + 0.078\ 42\Gamma_G\Gamma_L^4 + \Gamma_L^5)^{1/5}. \tag{8}$$

The main advantage of the second approach is that it is relatively easy (compared to the mixing parameter) to relate the FWHM parameters to the instrument resolution and specimen broadening effects.

The Gaussian and Lorentzian profile shapes are different enough (Figure 2) that it takes only a little practice to identify the major contribution to one's own X-ray diffraction peaks. The peaks from our laboratory instruments have been principally Lorentzian (Figure 3). The proportion of Gaussian and Lorentzian generally varies with angle. The peaks become more Lorentzian at high angles because they become dominated by the Cu $K\alpha$ emission profile. This variation in shape with angle leads to complicated profile functions.

As we have seen, several factors contribute to low-angle asymmetry of X-ray diffraction peaks. Rietveld (1969) used a simple model to describe the asymmetry of his broad neutron diffraction peaks. GSAS profile function 2 uses another simple model for asymmetry derived by Howard (1982), and this model works well for X-ray data as long as the peaks are

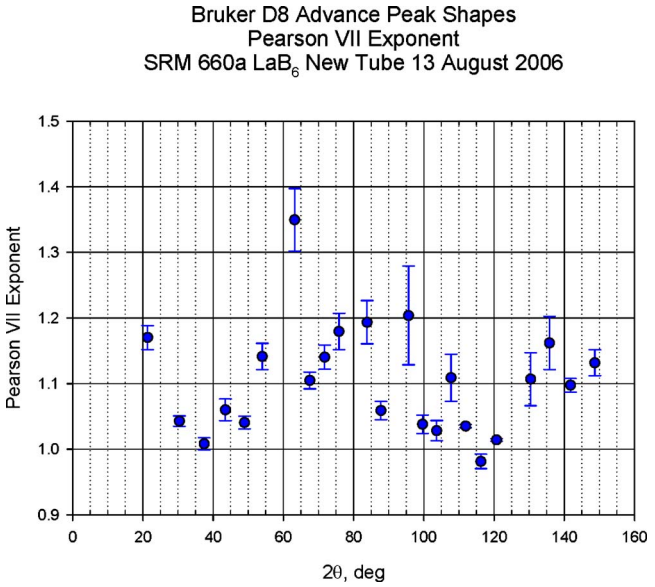

Figure 3. (Color online) The shapes of NIST SRM 660a LaB_6 measured on a Bruker D8 Advance diffractometer equipped with a VÅNTEC-1 position-sensitive detector. Each peak doublet was fitted using Pearson VII profiles with the program SHADOW. An exponent of 1 in a Pearson VII function corresponds to a Lorentzian peak shape, while larger exponents result in profiles which are more Gaussian. The values slightly >1 indicate that the peaks are mainly Lorentzian in character, and thus the instrument profile function should be dominated by the Lorentzian terms X and Y (Tables II and III).

not too asymmetric. The asymmetry of X-ray peaks is generally dominated by the axial divergence contribution. Finger *et al.* (1994), based on an analysis by van Laar and Yelon (1984), developed a more fundamental model for this asymmetry. The key parameters are S/L=the sample "half height"/diffractometer radius and H/L=the slit half height/diffractometer radius. S/L and H/L are refinable parameters but can be calculated from the diffractometer geometry and then fixed. In practice, it is often the length of the filament in the X-ray tube and the divergence of the Soller slits that are more important since the specimens and the lengths of the receiving slits are longer than the filament length.

In addition to parameters describing the peak shapes, Rietveld profile functions often include parameters to model changes in peak positions. These include a diffractometer zero and terms for specimen displacement and transparency.

Peaks from real materials almost always contain specimen contributions to the profiles. The major effects are size and microstrain broadening. The simplest way to visualize size broadening is to remember that diffraction is an interference phenomenon, and fewer slits in a diffraction grating (smaller crystallite) result in a fuzzier diffraction pattern (broader peaks). The mathematical treatment, conveniently summarized by Scardi (2008), involves the integral breadth of a peak, and ultimately the Scherrer equation

$$\beta(2\theta) = \frac{\lambda K_\beta}{D \cos\theta} \tag{9}$$

falls out naturally. The symbol β is the integral breadth (the integrated area divided by the peak height), λ is the wavelength, K_β is a constant which depends on the shape of the crystallites [JAK has always used 0.89 (Warren, 1990)], and D is the crystallite size (strictly speaking, the "column length"). Our experience is that size broadening is almost always Lorentzian. Rietveld programs include a Lorentzian term such as $X/\cos\theta$ (sometimes with a different letter) in the profile function to describe size broadening as well as part of the instrumental Lorentzian component of the profiles. A lognormal distribution is appropriate for many normal powders (Scardi and Leoni, 2001; Langford *et al.*, 2000). This function results in a range of particle sizes and thus a dominant Lorentzian character to the size broadening. Only rarely is Gaussian size broadening observed; this requires a very tight monodisperse distribution, which is rarely encountered in powder specimens (but is sometimes seen in polycrystalline solid specimens such as pieces of metal).

Microstrain broadening ultimately arises from local variations in the lattice parameters, which are the result of imperfections in the crystal structure. The easiest way to visualize the effect of microstrain broadening is to consider the differential of the Bragg equation (Scardi, 2008). Ultimately microstrain contribution to the profiles is a function of $\tan\theta$, so the Rietveld profile functions include a term such as $Y\tan\theta$ (which also describes the Cu $K\alpha$ line shape). Our experience is that microstrain broadening is almost always Lorentzian. Microstrain broadening is often anisotropic, so the more elaborate description of Stephens (1999) is incorporated into most Rietveld programs.

GSAS profile function 2 includes Gaussian [Eq. (10)] and Lorentzian [Eq. (11)] components of the pseudo-Voigt function separately (to model the variation in shape with angle), as well as terms which shift the peak positions [Eq. (12)],

$$\sigma^2 = U\tan^2\theta + V\tan\theta + W + \frac{P}{\cos^2\theta}, \tag{10}$$

$$\gamma = \frac{X + \text{ptec}\cos\varphi}{\cos\theta} + (Y + \text{stec}\cos\varphi)\tan\theta, \tag{11}$$

$$\Delta 2\theta = \text{zero} + \left(\frac{f_i\text{asym}}{\tan 2\theta}\right) + \text{shft}\cos\theta + \text{trns}\sin 2\theta. \tag{12}$$

The symbol σ is the variance of the Gaussian portion of the pseudo-Voigt profile and γ is the Lorentzian FWHM. The "ptec" and "stec" terms are anisotropic size and strain broadening coefficients for reflections which make an angle φ with a user-defined unique axis, and f_i is a constant calculated by GSAS. Profile functions 3–5 include the Finger asymmetry model and the Stephens anisotropic broadening model.

III. EXPERIMENTAL

An instrumental profile function is determined by measuring the pattern of a sample known (or assumed) to exhibit no size or strain broadening over as wide an angular range as the diffractometer will permit. The sample is generally a NIST SRM. The parameters discussed below were determined from patterns measured using SRM 660a (LaB_6), SRM 1976a (corundum plate), or their predecessors. Silicon SRM 640b and its predecessors exhibited significant microstrain broadening as well as granularity and so were not suit-

TABLE II. GSAS function 2 instrument profile parameters for a variety of laboratory diffractometers.

Diffractometer	Date	*U*	*V*	*W*	*X*	*Y*	Asym
X'Pert Pro PIXcel/0.04 rad Soller	08/2010	0.8048	0	0.5103	2.537	1.946	4.343
D2/Lynxeye	05/2010	1.371	0	2.393	2.183	1.199	2.774
D2/Lynxeye	10/2009	2.8329	0	2.695	1.853	2.488	2.194
X'Pert Pro PIXcel/mono	01/2008	0.7565	0	3.646	2.428	1.902	1.063
X'Pert Pro PIXcel/no mon	01/2008	2.6369	0	0	2.778	0	2.486
D8/VANTEC	04/2004	0.2879	0	1.124	2.477	2.103	2.052
PAD V	06/2007	1.0270	0	6.640	1.237	2.693	2.109
D/MAX-B	06/2002	0.567	0	18.680	2.301	1.960	6.048
Miniflex	09/2001	5.568	0	20.47	3.614	0	5.487
PW17xx	08/1998	0	0	5.217	0	9.77	7.603

able. The newer versions 640c and 640d do not have these problems and so are useful for determining the instrumental profiles.

A Rietveld refinement is then carried out using a previous instrument parameter file or a generic template. The file *inst_xry.prm* supplied with GSAS is a good enough start for most laboratory diffractometers. Unlike most Rietveld refinements, the lattice parameters are fixed; NIST determined them for us, and we do not want to refine them!

Refinements to determine the instrument parameters can include as many variables as necessary to model the pattern adequately. It may be necessary to refine the structural model (atom coordinates and displacement coefficients) to fit the relative peak intensities well. In such a refinement it may be appropriate to refine the diffractometer zero, depending on the type and alignment of the diffractometer. We expect this value to be small since the pattern was measured after a mechanical alignment of the diffractometer. Once this value is determined, it is fixed for this instrument configuration and does not need to be refined for real samples. Real systematic peak position errors in the Bragg-Brentano geometry result from specimen displacement and transparency; in particular, for most refinements of inorganic materials the dominant systematic error to be refined is displacement. However, for the Debye-Scherrer diffractometers (including most synchrotron instruments), the zero point is often less well defined and may need to be refined for real samples.

We find it useful to collect the pattern from a low angle, to permit modeling of the low-angle background, and to give an idea of what background function and how many coefficients to expect in refinements on real samples. Such background functions derived for an SRM are, however, only approximations to those for real specimens as there are several specimen-dependent contributions to the background (Riello *et al.*, 1995). We use empirical background functions because there is no universal physically based background function.

The most effort in such a refinement goes into determining the profile coefficients. The profile coefficients are often highly correlated, so damping is sometimes necessary. It is always wise to turn on output of the correlation coefficients if not done by default. Because the differences in the shapes are mainly in the tails, it is wise to use a wide peak wing cutoff, say 0.1% or less of the maximum intensity. Because the peaks are narrow, we expect all of the coefficients to be small numbers.

Different instrument configurations, particularly the size of the divergence slit and the divergence of the Soller slits, affect the profile coefficients greatly. A different instrument parameter file needs to be generated for each instrument configuration used in the laboratory.

IV. DISCUSSION

Instrument parameters (GSAS profile function 2) for a number of laboratory diffractometers are reported in Table II. It is important to note that these parameters *do not* reflect the relative quality of the instruments. By adjustment of the optical configurations, any instrument can be made to yield profiles like any other. The configurations of these instruments were, however, not very different from the default setups by the manufacturers. When different, the configurations were in the direction of higher resolution and more-symmetric peak shapes (for example, 0.02 rad Soller slits on the X'Pert Pro rather than the default 0.04 rad). Adding a

TABLE III. GSAS function 3 instrument profile parameters for a variety of laboratory diffractometers.

Diffractometer	*U*	*V*	*W*	*X*	*Y*	*S*/*L*	*H*/*L*
X'Pert Pro PIXcel/0.04 rad Soller	1.423	0	0.5061	2.842	1.509	0.035 47	0.005 22
D2/Lynxeye	1.376	0	2.640	2.410	0.850	0.029 51	0.0005
X'Pert Pro PIXcel/mono	1.153	−0.928	4.161	2.472	1.814	0.015 77	0.0005
X'Pert Pro PIXcel/no mon	2.314	0	0	3.040	0	0.027 88	0.0005
D8/VÅNTEC	0.3365	0	1.032	2.526	2.051	0.026 95	0.0005
PAD V	1.103	0	6.412	1.173	2.842	0.030 18	0.0005
D/MAX-B	3.219	−7.822	24.370	2.460	1.609	0.038 58	0.0005

Note: In all of these profile functions, $P=0$.

TABLE IV. GSAS profile 2 functions for several synchrotron diffractometers.

Instrument	Date	U	V	W	X	Y	Asym
APS 5-BM-C	10/2002	0.1	0	0	0.2505	0.9462	0
APS 5-BM-C	08/2006	17.1	−8.8	1.3	0	0	0
APS 1-ID	02/2002	0.1	0	0	0.2505	0.9462	0.0646
APS 10-ID-B	01/2000	0.3540	0	0.2908	0.3565	0.5177	0.4744
APS 32-ID	12/2004	0.3120	0	0.0104	0.1186	0.4062	0.0419
LNLS D10B		0.8777	−0.1600	0.1063	0.7604	1.1904	0.5157
NSLS X3B1	03/2004	6.427	−1.067	0	0.6102	0.6796	0.6733

diffracted beam monochromator to the X'Pert Pro changed the profile shapes significantly.

The modern high-resolution instruments have remarkably similar profile functions. U ranges from 0 to 3, W from 0 to 4, X from 1 to 3, Y from 0 to 3, and "asym" from 1to 3. (The units vary with the coefficient.) V is zero for all of these instruments. In our experience, V tends to be a negative number that often refines to a slightly positive value and/or one insignificantly different from zero, so it was fixed at zero in all of the refinements. The relative standard uncertainties on most of these coefficients are rather high, often in the first decimal place. Our practice has been to include all of the significant figures in the instrument parameter file. The older smaller-radius instruments tended to yield broader peaks (larger coefficients), and their shorter Soller slits resulted in higher values for the asymmetry parameter.

Each of the refinements also included a specimen displacement coefficient and the diffractometer zero, but these values are not reported here as they depend on the details of the alignment and the specimen packing and mounting. Although we do not expect specimen transparency to be important for LaB_6 using Cu $K\alpha$ radiation, some of the refinements also included a transparency term to model very small systematic errors in peak positions, errors which probably arise from subtle goniometer errors.

For some of the instruments, we also generated parameters (Table III) for GSAS profile function 3, which incorporates the Finger asymmetry model. The shape parameters refined to values similar to those for profile function 2. Because for all of these instruments the specimens and the lengths (not the widths) of the receiving slits were larger than the filament length (12 mm in all cases), the values of the symmetry parameters S/L and H/L can be estimated by dividing 6 mm into the goniometer radius (240, 217.5, and 210 mm for the X'Pert Pro, D8, and PAD V, respectively) to obtain values of 0.0250, 0.0276, and 0.0286. Refinement of both coefficients simultaneously tends to yield one reasonable value and one value below zero, which GSAS resets to 0.0005.

In our experience, size and microstrain broadening are almost always Lorentzian, so we tend to fix U, V, W, asym, S/L, and H/L at the instrumental values and refine only X and Y [or the $S(hkl)$ coefficients of the Stephens model]. On the rare occasions we observe the Gaussian strain broadening (judged by looking at the fit to the peaks) we include U in the refinement. On the even rarer occasions when size broadening is Gaussian, the P coefficient can be refined successfully.

Although these parameters were generated using GSAS, they can be converted easily into their FULLPROF (Rodriguez-Carvajal, 2001) equivalents. These conversions are based on the different definitions of the Thompson-Cox-Hastings pseudo-Voigt function used by the programs, as documented in the respective manuals. For the Gaussian parameters, the conversion factor is 1803.4, which is equivalent to a conversion from centidegrees squared divided by $8 \times \ln(2)$. For the Lorentzian parameters, the conversion factor is 100, equivalent to conversion from degrees to centidegrees, and the letter symbols are interchanged. The Finger-Cox-Jephcoat asymmetry parameters are equivalent in the two programs. The individual conversions are

$$GU(\text{GSAS}) = 1803.4U(\text{FULLPROF}), \tag{13}$$

$$GV(\text{GSAS}) = 1803.4V(\text{FULLPROF}), \tag{14}$$

$$GW(\text{GSAS}) = 1803.4W(\text{FULLPROF}), \tag{15}$$

$$GP(\text{GSAS}) = 1803.4\text{I}G(\text{FULLPROF}), \tag{16}$$

$$LX(\text{GSAS}) = 100Y(\text{FULLPROF}), \tag{17}$$

$$LY(\text{GSAS}) = 100X(\text{FULLPROF}), \tag{18}$$

$$S/L(\text{GSAS}) = S\_L(\text{FULLPROF}), \tag{19}$$

$$H/L(\text{GSAS}) = D\_L(\text{FULLPROF}). \tag{20}$$

Instrument parameter files are also critical to interpreting synchrotron data, and profile functions for several beamlines are reported in Tables IV and V. Most of these beamlines have similar optical configurations (Si double crystal monochromators and analyzer crystals), so we might expect the line profiles to be similar. Indeed, the parameters listed for APS beamline 5-BM-C were also supplied by several other beamlines, so some "trading" of parameters has occurred. Most of the parameters for APS and NSLS beamlines were generated by us. The profile parameters seem independent of wavelength, which ranges from 0.15 to 1.20 Å (10 to 80 keV) among these instruments. This observation perhaps should not be surprising as Caglioti's analysis involves monochromator characteristics and the collimation but not the wavelength.

As we expect, the synchrotron peaks are narrower than those from laboratory instruments. Because the Lorentzian shape of a characteristic emission profile is not involved in the convolutions, the synchrotron instrumental peak shapes tend to be more Gaussian than those of laboratory instru-

TABLE V. GSAS profile 3 instrument parameters for several synchrotron diffractometers.

Instrument	Date	U	V	W	P	X	Y	S/L	H/L
APS 5-BM-C	10/2002	1.212	0	0	0	1.980	0	0.001 353	0.007 183
APS 1-ID	02/2002	0.1	0	0	0	0.1845	11.190	0.0005	0.004 587
APS 10-ID	10/2003	1.212	0	0	0	0.198	0	0.001 353	0.007 183
APS 11-BM-B	02/2009	1.163	−0.126	0.063	0	0.173	0	0.001 10	0.001 10
APS 32-ID	12/2004	1.212	0	0	0	0.198	0	0.001 353	0.007 183
AS PD		0.0522	0.5640	0.0621	0	0.293	0.171		
NSLS X7B MAR345		0	−125.9	73.3	0	2.03	0	0.0001	0.1000
NSLS X16C		0	0	0	1	3	30	0.014	0.014

ments. Our experience is that size and microstrain broadening are Lorentzian on synchrotron instruments.

For well-characterized instrument profiles on these similar instruments, the coefficients fall in the ranges $0<U<1.2$, $-1<V<0$, $0<W<1$, $0<X<1$, $0<Y<1$, $0<\text{asym}<0.5$, $0<S/L<0.001$, and $0<H/L<0.007$. Insertion device beamlines tend to have more-symmetric peaks than bending magnet lines. Synchrotron users tend to prefer GSAS profile functions 3 and 4 because the Finger model describes the asymmetry better than the simpler Howard model.

NSLS beamline X7B has a very different optical configuration than the others. It uses a double Laue monochromator and a MAR345 image plate detector. We can therefore expect and observe a very different instrument profile function.

After the refinement to determine the instrument parameters, a new instrument parameter file is generated most conveniently by using the *instedit* function of the Powder menu in EXPGUI (Toby, 2001). The ASCII parameter files can also be copied and edited by hand.

ACKNOWLEDGMENTS

The authors thank Kia Wallwork (Australian Synchrotron powder beamline), Eduardo Granado (LNLS D10B), Jonathan Hanson (NSLS X7B), and Peter W. Stephens (NSLS X16C) for supplying instrument parameter files for their beamlines.

Caglioti, G., Paoletti, A., and Ricci, F. P. (**1958**). "Choice of collimators for a crystal spectrometer for neutron diffraction," Nucl. Instrum. **3**, 223–228.

Cheary, R. W. and Cline, J. P. (**1995**). "An analysis of the effect of different instrumental conditions on the shapes of X-ray line profiles," Adv. X-Ray Anal. **39**, 75–82.

Cheary, R. W. and Coelho, A. (**1992**). "A fundamental parameters approach to X-ray line profile fitting," J. Appl. Crystallogr. **25**, 109–121.

Cranswick, L. M. D. (**2008**). *Powder Diffraction: Theory and Practice*, edited by R. E. Dinnebier and S. J. L. Billinge (RSC, Cambridge), pp. 134–165.

Finger, L. W., Cox, D. E., and Jephcoat, A. P. (**1994**). "A correction for powder diffraction peak asymmetry due to axial divergence," J. Appl. Crystallogr. **27**, 892–900.

Hartwig, J., Hölzer, G., Wolf, J., and Förster, E. (**1993**). "Remeasurement of the profile of the characteristic Cu K_α emission line with high precision and accuracy," J. Appl. Crystallogr. **26**, 539–548.

Howard, C. J. (**1982**). "The approximation of asymmetric neutron powder diffraction peaks by sums of Gaussians," J. Appl. Crystallogr. **15**, 615–620.

Kern, A. (**2008**). *Principles and Applications of Powder Diffraction*, edited by A. Clearfield, J. Reibenspies, and N. Bhuvanesh (Wiley, Chichester, U.K.), pp. 158–198.

Klug, H. P. and Alexander, L. E. (**1974**). *X-Ray Diffraction Procedures for Polycrystalline and Amorphous Materials*, 2nd ed. (Wiley, New York).

Langford, J. I., Louër, D., and Scardi, P. (**2000**). "Effect of a crystallite size distribution on X-ray diffraction line profiles and whole-powder-pattern fitting," J. Appl. Crystallogr. **33**, 964–974.

Larson, A. C. and Von Dreele, R. B. (**2004**). *General Structure Analysis System (GSAS) (Report No. LAUR 86-748)* (Los Alamos National Laboratory, Los Alamos, NM).

Le Bail, A. (**2008**). *Powder Diffraction: Theory and Practice*, edited by R. E. Dinnebier and S. J. L. Billinge (RSC, Cambridge), pp. 134–165.

Masson, O., Dooryhee, E., and Fitch, A. N. (**2003**). "Instrument line-profile synthesis in high-resolution synchrotron powder diffraction," J. Appl. Crystallogr. **36**, 286–294.

Riello, P., Fagherazzi, G., Clemente, D., and Canton, P. (**1995**). "X-ray Rietveld analysis with a physically based background," J. Appl. Crystallogr. **28**, 115–120.

Rietveld, H. (**1969**). "A profile refinement method for nuclear and magnetic structures," J. Appl. Crystallogr. **2**, 65–71.

Rodriguez-Carvajal, J. (**2001**). "Recent developments of the program FULLPROF," IUCR Newsl. **26**, 12–19.

Scardi, P. (**2008**). *Powder Diffraction: Theory and Practice*, edited by R. E. Dinnebier and S. J. L. Billinge (RSC, Cambridge), pp. 376–413.

Scardi, P. and Leoni, M. (**2001**). "Diffraction line profiles for polydisperse crystalline systems," Acta Crystallogr., Sect. A: Found. Crystallogr. **57**, 604–613.

Stephens, P. W. (**1999**). "Phenomenological model of anisotropic peak broadening in powder diffraction," J. Appl. Crystallogr. **32**, 281–289.

Thompson, P., Cox, D. E., and Hastings, J. B. (**1987**). "Rietveld refinement of Debye-Scherrer synchrotron X-ray data from Al_2O_3," J. Appl. Crystallogr. **20**, 79–83.

Toby, B. H. (**2001**). "*EXPGUI*, a graphical user interface for *GSAS*," J. Appl. Crystallogr. **34**, 210–213.

van Laar, B. and Yelon, W. B. (**1984**). "The peak in neutron powder diffraction," J. Appl. Crystallogr. **17**, 47–54.

Warren, B. E. (**1990**). *X-Ray Diffraction* (Dover, New York), pp. 251–254.

Wikipedia. (**2010**). "Convolution," ⟨http://en.wikipedia.org/wiki/Convolution⟩.

Young, R. A. (**1993**). *The Rietveld Method*, edited by R. A. Young (Oxford University Press, Oxford), pp. 7–10.

Young, R. A. and Wiles, D. B. (**1982**). "Profile shape functions in Rietveld refinements," J. Appl. Crystallogr. **15**, 430–438.